Single-electron spin decoherence by nuclear spin bath: Linked-cluster expansion approach

S. K. Saikin,[1,2,*] Wang Yao,[1,†] and L. J. Sham[1]

[1]*Department of Physics, University of California San Diego, La Jolla, California 92093-0319, USA*
[2]*Department of Physics, Kazan State University, Kazan 420008, Russian Federation*

We develop a theory for decoherence dynamics of a single-electron spin interacting with a nuclear spin bath. The approach yields a simple diagrammatic representation and analytical expressions of different nuclear spin excitation processes contributing to electron spin decoherence and dynamical phase fluctuations. It accounts for nuclear spin dynamics beyond the recently developed pair correlation models. As an illustration of the theory, we evaluated the coherence dynamics of a P donor electron spin in a Si crystal.

PACS number(s): 76.60.Lz, 03.65.Yz, 76.30.−v, 76.70.Dx

I. INTRODUCTION

An electron-nuclear spin coupling substantially affects electron spin dynamics in solids. This phenomenon is widely utilized in EPR probing of material structures.[1] However, for quantum technology applications of the electron spins[2,3] the coupling to nuclear spins as a source of relaxation and decoherence[4–8] has become a key issue. Entanglement of an electron spin with a nuclear spin bath results in an irreversible loss of coherence. Unlike spin relaxation,[7] the decoherence process is not suppressed even in strong magnetic fields. There are several methods to reduce the effects of spin bath, such as isotope purification,[9] dynamical polarization of nuclear spins, or dynamical decoupling of an electron spin evolution.[10] However, it is not clear if experimentally achievable values of isotope purification, nuclear polarization or precision of electron spin control are sufficient to suppress the effects of spin bath above the required threshold limit.[11] Moreover, for some technologically important materials these methods may be inapplicable. For example, isotope purification cannot be used in GaAs nanostructures, because all the stable isotopes (^{69}Ga, ^{71}Ga, ^{75}As) have nonzero nuclear spins. In this context theoretical models of electron-nuclear spin dynamics can provide a better understanding of electron spin decoherence processes and, hence, help in estimating and enhancing the effectiveness of coherence control schemes.

In this work we investigate the dynamics of a localized electron spin interacting with a nuclear spin bath in the low-temperature–high-field regime where the thermal energy is smaller than the electron Zeeman splitting. In this case the electron spin relaxation and decoherence due to phonon absorption[12] is suppressed. We also assume that the external field is high enough to prevent electron spin relaxation due to direct electron-nuclear spin flip-flop processes without phonon assistance.[13] Such a system possesses a long spin relaxation time that is crucial to quantum computing. Until recently, this problem has been studied using stochastic models of spectral diffusion.[14–16] Results of these works were verified by numerous experiments carried out on macroscopic samples. Recently, emphasis of experimental and theoretical studies has been shifted to the dynamics of single quantum systems, where stochastic models are inappropriate. Several analytical and numerical approaches based on quantum dynamics have been developed and used to investigate different aspects of the problem.[13,17–30] Among the issues addressed in

these studies are spin relaxation at low external fields,[18,19] effects of nuclear spin polarization on electron spin dynamics,[30] dynamical control for spin decoherence,[29] contributions of high order nuclear spin correlations into an electron spin echo,[28] etc. However, many questions are still open. How do stochastic and dynamical models relate to each other? How does one characterize short time qubit evolution?[31] What are the reversible and irreversible parts of spin dynamics?[32] What are the relative contributions of correlated nuclear spin clusters of different sizes in electron spin dynamics? How do nuclear spin correlations grow in time?[33]

Here, we demonstrate that diagram techniques developed previously in studies of Heisenberg ferromagnets[34–42] can be applied to evaluate the effects of a nuclear spin bath on a single-electron spin in the high field regime. Our theoretical approach provides a transparent representation of different nuclear spin dynamical processes contributing to the electron spin evolution. It naturally accounts for nuclear spin excitations beyond the pair correlation models. We show that the transverse evolution of an electron spin can be factorized to a precession in a nuclear Overhauser field and more complex dynamics due to electron-nuclear spin entanglement.[26] A conventional Hahn echo experiment cancels the phase due to precession in the nuclear field and also suppresses entanglement with the nuclear bath. As an illustration, we consider the dynamics of an electron spin localized at a phosphorous donor impurity in a Si crystal. We estimate the contributions of two, three, and four nuclear spin excitations to the electron spin decoherence and discuss the effects of Hahn echo on the spin decoherence.

The structure of the paper is as follows. In the next section we describe the starting Hamiltonian and discuss the assumptions used. Section III is devoted to diagrammatic representation of the decoherence process. In Sec. IV we discuss the approach and consider an example of the P donor electron spin in a Si crystal. Section V gives the conclusion. Appendix A contains the spin diagrammatic rules, Appendix B some specific properties of the linked cluster expansion for spin systems, and Appendix C explicit analytical expressions of some high order nuclear spin contributions to the electron spin dynamics.

II. MODEL

We consider the spin of a single electron localized in a quantum dot or bounded by a donor impurity. We assume

that only one type of nuclear spins with $I=1/2$ is present, though this assumption can be relaxed with the approach used. In a strong external magnetic field the effective Hamiltonian for a single-electron spin coupled by the contact hyperfine interaction[45] with a system of nuclei is derived from the first principles Hamiltonian by eliminating the electron spin-flip terms

$$H = \omega_e S^z - \omega_I \sum_i I_i^z + S^z \sum_i A_i^{\text{hf}} I_i^z + 2S^z \sum_{i \neq j} B_{ij}^{\text{hf}} I_i^+ I_j^-$$
$$+ \sum_{i \neq j} \{A_{ij}^{\text{dd}} I_i^z I_j^z + B_{ij}^{\text{dd}} I_i^+ I_j^-\}. \tag{1}$$

A similar Hamiltonian has been used in previous studies of the spectral diffusion problem.[24,26] The first two terms in Eq. (1) account for the electron and nuclear Zeeman energy level splittings in an external field H with the respective Larmor frequencies $\omega_e = g^* \beta H / \hbar$ and $\omega_I = \gamma H$. The z axis is chosen along the magnetic field. The third and fourth terms originate from the contact hyperfine interaction. In a strong magnetic field direct electron-nuclear flip-flop transitions $(S^+ I_i^- + S^- I_i^+)$ are forbidden by the energy conservation law. Therefore, beside a small visibility loss,[25] this part of the contact interaction contributes in second order to the effective coupling between nuclear spins [fourth term in Eq. (1)] only.[26] The coupling coefficients are $A_i^{\text{hf}} = (8/3)\pi g_e \beta \gamma |\Psi(R_i)|^2$ and $B_{ij}^{\text{hf}} = A_i^{\text{hf}} A_j^{\text{hf}} / 2\omega_e$, where $g_e = 2$ and g^* are the free and effective electron g factors, β is the Bohr magneton, γ is the nuclear gyromagnetic ratio, and $\Psi(R_i)$ is the electron wave function at the position of ith nuclear spin. The last term in Eq. (1) represents the secular part of the nuclear spin dipole-dipole interaction. For the electron nuclear spin interaction, we consider only the isotropic contact part. This is justified in cases where the dipolar e-n spin coupling is much weaker than the Fermi contact term, for example, for most of the Si sites around a shallow donor in silicon.[43] For the hyperfine interaction in the semiconductor quantum dots there are no available experimental data, but numerical estimates within the tight-binding model[44] confirm our assumption. In general, in a high field regime the dipolar e-n spin interaction contribute to the third and fourth terms in Eq. (1). It also results in spin echo envelope modulation,[46–49] through the $S^z I^\pm$ terms. The latter effect has been discussed elsewhere.[50] The effective Hamiltonian (1) is diagonal in the electron spin. Therefore, the nuclear spin bath affects the transverse electron spin dynamics only.

The initial state of the electron spin plus the system of nuclear spins is described by the density matrix $\rho(0)$ at the time moment, $t=0$, when the electron spin state has been prepared. Two assumptions are applied to $\rho(0)$. First, we use the standard approximation of a factorized system and bath[51] $\rho(0) = \rho_s^0 \otimes \rho_n^0$. The electron spin is initially prepared in the pure state $(1/\sqrt{2})(|+\rangle + |-\rangle)$, e.g., by a $\pi/2$ pulse. The second assumption is that the nuclear spin system is in a pure state that is an eigenstate of $\Sigma_i I_i^z$ operator. With the latter statement we neglect the nuclear spin-spin correlations at $t<0$. Influence of different initial states of the nuclear bath on the electron spin evolution has been discussed in Refs. 20 and 23 though the lack of the nuclear spin-spin interaction in these

papers may affect their conclusions. It has been argued that the pure spin state utilized here can be useful for quantum computation purposes because it does not destroy the electron spin coherence at short time scales. After statistical averaging over possible initial configurations the nuclear spin density matrix is $\rho_n^0 = \Sigma p_n |n\rangle\langle n|$, where p_n is the statistical weight of a given nuclear configuration $|n\rangle = |\uparrow \uparrow \downarrow \uparrow \downarrow \downarrow \dots\rangle$.

The evolution of the up-down component $(+-)$ of an electron spin density matrix can be written as[26]

$$\rho_{+-}(t) = \rho_{+-}^0 e^{-i\omega_e t} \text{Tr}_n \{e^{-i(H_0+V_+)t} \rho_n^0 e^{i(-H_0+V_-)t}\}, \tag{2}$$

where

$$H_0 = (1/2) \sum_i A_i^{\text{hf}} I_i^z,$$

$$V_\pm = V_{\text{dd}} \pm V_{\text{hf}},$$

$$V_{\text{dd}} = \sum_{i \neq j} \{A_{ij}^{\text{dd}} I_i^z I_j^z + B_{ij}^{\text{dd}} I_i^+ I_j^-\},$$

$$V_{\text{hf}} = \sum_{i \neq j} B_{ij}^{\text{hf}} I_i^+ I_j^-. \tag{3}$$

Here, we used the fact that the Hamiltonian (1) commutes with S_z and projected it to the electron spin-up $(+)$ and spin-down $(-)$ subspaces. The projected operators are written as two terms, H_0, which is a sum of single spin operators, and $V_\pm$, which describes spin-spin interactions. A contribution of the nuclear Zeeman splitting, the second term in Eq. (1), is cancelled, because it commutes with the rest of the Hamiltonian. If the nuclear Larmor frequency ω_I varies from site to site due to the inhomogeneity of the external field or other factors, then its fluctuating part should be included in H_0. Below, we will keep the superscript indexes (hf) and (dd) in the coupling constants only if it is not clear from the context what type of interaction is used.

By the relations

$$e^{-i(H_0+V_+)t} = T\{e^{-i\int_0^t V_+(t'-t)dt'}\}e^{-iH_0 t},$$

$$e^{-i(H_0-V_-)t} = e^{-iH_0 t} T\{e^{i\int_0^t V_-(t')dt'}\}, \tag{4}$$

where $T\{\cdots\}$ is a time ordering operator, and our assumption on the initial nuclear spin density matrix, Eq. (2) is transformed to

$$\rho_{+-}(t) = \rho_{+-}^0 e^{-i\omega_e t}$$
$$\times \sum_n p_n e^{-i\omega_n t} \langle n| T\{e^{i\int_0^t V_-(t')dt'}\} T\{e^{-i\int_0^t V_+(t'-t)dt'}\} |n\rangle, \tag{5}$$

where $\omega_n = \langle n|2H_0|n\rangle$ is a contribution of the nuclear Overhauser field to the electron spin precession frequency and $V_\pm(t)$ is $V_\pm$ in the interaction picture defined by H_0. For a single shot measurement of the single-electron spin, the nuclear bath contributes to the shift of the electron precession frequency ω_n determined by the initial configuration, and to the complicated dynamics due to coupling between

nuclear spins that is described by the bracket $\langle n|\cdots|n\rangle$. The weight factor p_n corresponds to a statistical averaging over an ensemble of electron spins or repeated measurements. For an ensemble measurement, Eq. (5) describes a free induction decay[45] (FID), where the transverse magnetic moment decays due to an inhomogeneous distribution of spin precession frequencies and also due to the spectral diffusion in the presence of the nuclear spin environment. Equation (5) can be viewed as an exact formal solution for the electron spin dynamics. In the following sections we will evaluate the term in it between the angular brackets using the linked-cluster expansion (LCE) formalism.[52,53]

In Eq. (5) the product of two exponential operators can be transformed to a single exponential form $T\{e^{-i\int_{-t}^{t}\tilde{V}(t')dt'}\}$ by shifting the time variable $t'-t\rightarrow t'$ in the second exponent. One can see that in this case the potential $\tilde{V}(t')$ is continuous for the hyperfine-mediated interaction given by Eq. (3), while for the dipole-dipole nuclear spin-spin interactions it changes sign at $t'=0$. To avoid operations with discontinuous potentials we will use the two-exponential form between the brackets in Eq. (5) keeping in mind that it can be transformed to a single exponent.

Schematically, the brackets in Eq. (5) can be shown as a two branch propagation, see Fig. 1. The system propagates on the first branch with the Hamiltonian $V_+(t'-t)$ and after that on the second branch with $-V_-(t')$. This is similar to the
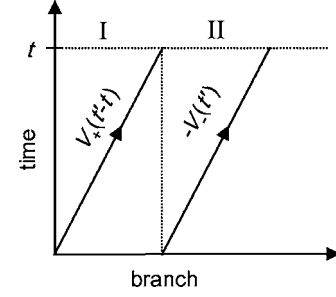
FIG. 1. A schematic representation of the two-branch evolution.

nonequilibrium Green's function approach.[54,55]

The factorization of the nuclear spin induced dynamics to the phase factor acquired in the nuclear Overhauser field and the complex dynamics due to entanglement between bath modes is consistent with EPR experiments. For example, see Ref. 56, where an electron spin resonance line broadening can be resolved to inhomogeneous and homogeneous parts.

The above procedure also can be applied to evaluate electron spin dynamics in experiments where the electron spin is flipped by magnetic pulses. For example, for a Hahn spin echo ($\pi/2-t-\pi-t-$echo) the evolution equation can be written as

$$\rho_{+-}(2t) = -\rho_{-+}^0 \sum_n p_n \langle n|T\{e^{i\int_0^t V_+(t-t')dt'}\}T\{e^{i\int_0^t V_-(-t')dt'}\}T\{e^{-i\int_0^t V_+(t'-t)dt'}\}T\{e^{-i\int_0^t V_-(-t')dt'}\}|n\rangle. \tag{6}$$

We emphasize that the phase factor due to precession in the external field plus the nuclear field that appears in Eq. (5) is cancelled in the echo. Moreover, the bracket $\langle n|\cdots|n\rangle$ describing the electron-nuclear spin entanglement is different from the one in Eq. (5). These features correspond respectively to elimination of inhomogeneous broadening and suppression of spectral diffusion in ensemble measurements.[45]

III. LCE AND DECOHERENCE

Using LCE, we can write the expectation value of the time ordered exponent as[52,53]

$$\langle n|T\{e^{\int_0^t V(t')dt'}\}|n\rangle = e^{\langle V_1\rangle + \langle V_2\rangle + \langle V_3\rangle + \cdots}, \tag{7}$$

where $V(t')$ is an interaction and $\langle V_k\rangle$ is a contribution of *linked* diagrams[53] only to the integral

$$\int_0^t dt_1 \int_0^t dt_2 \cdots \int_0^t dt_k \langle n|T\{V(t_1)V(t_2)\cdots V(t_k)\}|n\rangle. \tag{8}$$

The coefficient $1/k$ that appears in LCE, is included in the $\langle V_k\rangle$ terms. This expansion provides a convenient exponential form to describe the dynamical processes. Moreover, each perturbation term $\langle V_k\rangle$ in it corresponds to an infinite

sum of terms in the conventional perturbation theory.

The expectation value in the expression (8) can be evaluated by a diagrammatic technique. The term $\langle V_k\rangle$ in Eq. (7) is of the kth order in the interaction. It describes the correlated dynamics of a cluster containing up to k spins. Because the proof of LCE can be given based on combinatorics,[53] the expansion procedure should be applicable to potentials, discontinuous in time, or to products of several evolution operators given in Eqs. (5) and (6).

Diagrammatic rules for spins are not so transparent as for fermions or bosons, because commutation brackets of spin operators do not yield c numbers. Many papers addressed this issue.[35–42] In our derivations we use the technique described in Refs. 38, 39, and 42 with modifications adapted for the specifics of the problem. A brief summary of this technique and the used diagrammatic representations are given in Appendix A.

The LCE expansion of the scattering matrix (7) can be described by the same series of diagrams as a free energy in Matsubara formalism given in Ref. 39. The two-exponential representation of the scattering matrix in Eq. (5) does not change the structure of the diagram series, but affects the spin propagators only. In Figs. 2–4 we show the sets of diagrams corresponding to the bracketed expression in
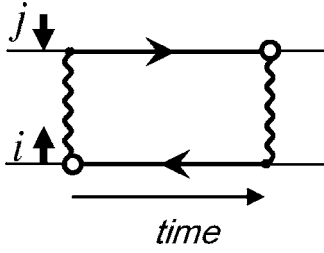
FIG. 2. A second order diagram corresponding to the nuclear spin pair flip-flop processes.

Eqs. (5) and (6) up to the fourth order in the nuclear spin-spin interaction.

We first discuss the scenario where the nuclear dynamics starts from a pure initial states. Ensemble results are obtained by taking statistical average of all possible initial configurations. Dynamics of each distinct configuration of spins in a cluster, in general, should be depicted by a different diagram specifying an initial spin configuration and the time arrow as shown in Fig. 2. However, in many cases analytical expressions for these configurations can be transformed to one another as is discussed in Appendix A. To reduce the number of diagrams in the figures, we omit the configuration dependence, taking one diagram to represent all possible configurations. In both analytical and numerical evaluations we calculate contributions of all distinct spin clusters. We also drop the time arrow for simplicity.

To evaluate diagrams given in Figs. 2–4 we use a 2×2 matrix (matrix elements indexing the branches shown in Fig. 1) Green's function at an ith site

$$\mathbf{K}^i(\tau) = e^{i\omega_i\tau}\begin{pmatrix} \delta_{i\downarrow}\theta(-\tau) - \delta_{i\uparrow}\theta(\tau) & \delta_{i\downarrow}e^{-i\omega_i t} \\ -\delta_{i\uparrow}e^{i\omega_i t} & \delta_{i\downarrow}\theta(-\tau) - \delta_{i\uparrow}\theta(\tau) \end{pmatrix},$$
(9)

where $\omega_i = A_i^{\mathrm{hf}}/2$ and $\tau = t_1 - t_2$. The total evolution time t appears in the off-diagonal elements of $\mathbf{K}^i(\tau)$. Matrix elements of the Green's function (9) have a simple physical meaning. The propagator starts at time t_1 on a branch denoted by a row index and ends at time t_2 on a branch denoted by a column index. To account for the two-branch propagation the spin-spin coupling coefficients $A_{ij}^{\mathrm{dd}}, B_{ij}^{\mathrm{dd}}$ should be multiplied by a σ_z Pauli matrix ($\mathbf{A}_{ij}^{\mathrm{dd}} = A_{ij}^{\mathrm{dd}}\sigma_z, \mathbf{B}_{ij}^{\mathrm{dd}} = B_{ij}^{\mathrm{dd}}\sigma_z$) and B_{ij}^{hf} should be multiplied by a 2×2 unit matrix ($\mathbf{B}_{ij}^{\mathrm{hf}} = B_{ij}^{\mathrm{hf}}\mathbf{1}$). In the analytical expressions for the diagrams one has to sum over repeated matrix indices in addition to integration over the time variables.

The first order linked cluster diagram corresponds to $\langle n|\mathbf{A}_{ij}^{\mathrm{dd}}I_i^z I_j^z|n\rangle$ (not shown in Figs. 2–4). However, its contribution vanishes because the sum over the branches is equal
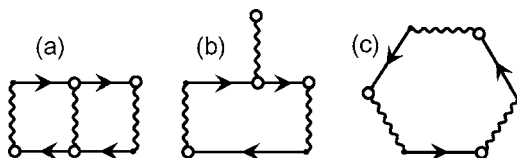
FIG. 3. A set of third order diagrams.
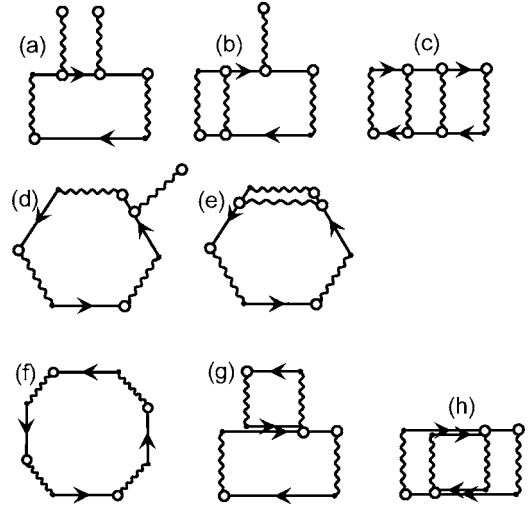
FIG. 4. Some fourth order diagrams.

to $\mathrm{Tr}\{\mathbf{A}_{ij}^{\mathrm{dd}}\}=0$. The first non-zero contribution to the decoherence process is given by the second order diagrams which represent nuclear pair-spin flips, Fig. 2. The corresponding analytical expressions are

$$\langle V_2^{\mathrm{hf}}\rangle = -\sum_{i=\uparrow,j=\downarrow} (B_{ij}^{\mathrm{hf}})^2\left\{\frac{2it}{\omega_{ij}} + \frac{1-e^{2i\omega_{ij}t}}{\omega_{ij}^2}\right\},$$
(10)

for the hyperfine-mediated interaction only, and

$$\langle V_2^{\mathrm{dd}}\rangle = -\sum_{i=\uparrow,j=\downarrow} (B_{ij}^{\mathrm{dd}})^2\left\{\frac{2it}{\omega_{ij}} + 4\frac{1-e^{i\omega_{ij}t}}{\omega_{ij}^2} - \frac{1-e^{2i\omega_{ij}t}}{\omega_{ij}^2}\right\},$$
(11)

for the dipole-dipole interaction only, where we define $\omega_{ij} = \omega_i - \omega_j$. This result is consistent with Ref. 26. The real parts of Eqs. (10) and (11) contribute to the electron spin decoherence while the imaginary parts renormalize the electron spin precession frequency and, hence, produce phase fluctuations. The $\langle V_2\rangle$ diagram with a cross-term $B^{\mathrm{hf}}B^{\mathrm{dd}}$ contribution of the dipole-dipole and hyperfine-mediated interactions is zero because the spin propagators over different branches cancel each other. Therefore, to the second order in the nuclear spin-spin interaction the contributions of these two mechanisms to electron spin dynamics are completely separable.

We emphasize that in comparison with the conventional perturbation expansion LCE converges faster. Each order in LCE corresponds to the sum of an infinite subseries. For example, the second order correction in LCE is a partial sum shown in Fig. 5. It includes a series of even orders of a perturbation expansion.

$$e^{\,\boxed{}} = 1 + \boxed{} + (1/2!)\,\boxed{}\,\boxed{} + \dots$$

FIG. 5. The second order contribution to decoherence in LCE which includes a series of even orders of a conventional perturbation expansion.

The third order diagrams in Fig. 3 can be divided into two groups. The first group includes diagrams 3(a), 3(b) and corresponds to $\langle V_2 \rangle$ diagram with attached $I_i^z I_j^z$ interaction lines.

$$\mathbf{K}^i(t_1, t_2) = e^{i\omega_i \tau} \begin{pmatrix} e^{i\Delta\omega_i \tau}[\delta_{i\downarrow}\theta(-\tau) - \delta_{i\uparrow}\theta(\tau)] & \delta_{i\downarrow}e^{-i\omega_i' t}e^{i\Delta\omega_i\theta} \\ -\delta_{i\uparrow}e^{i\omega_i' t}e^{-i\Delta\omega_i\theta} & e^{-i\Delta\omega_i\tau}(\delta_{i\downarrow}\theta(-\tau) - \delta_{i\uparrow}\theta(\tau)) \end{pmatrix}, \tag{12}$$

$\tau = t_1 - t_2$, $\theta = t_1 + t_2$, $\omega_i' = \omega_i + \Delta\omega_i$ and $\Delta\omega_i = \sum_j A_{ji}\langle I_j^z \rangle$. This modifies the dipole-dipole pair flip-flop term (11) as

$$\langle V_2^{\text{ren}} \rangle = - \sum_{i=\uparrow, j=\downarrow} (B_{ij}^{\text{dd}})^2 \left\{ \frac{it}{\omega_{11}} + \frac{it}{\omega_{22}} + \frac{1 - e^{i\omega_{11}t}}{\omega_{11}^2} + \frac{1 - e^{i\omega_{22}t}}{\omega_{22}^2} \right. \\ \left. + \frac{(1 - e^{i\omega_{11}t})(1 - e^{i\omega_{22}t})}{\omega_{11}\omega_{22}} \right\}, \tag{13}$$

where $\omega_{11} = \omega_{ij} + \Delta\omega_i - \Delta\omega_j$ and $\omega_{22} = \omega_{ij} - \Delta\omega_i + \Delta\omega_j$. If we assume that $\Delta\omega_i$ is independent of the site, then Eq. (13) transforms back to Eq. (11). Therefore, the contribution of these renormalization terms is reduced if the initial polarization of the nuclear spin bath is homogeneous. A similar modification of the pair flip-flop term can be due to an inhomogeneous distribution of the nuclear Larmor frequencies ω_I in Eq. (1). The diagram 3(a) contributes to the renormalization of a pair dynamics by $I^z I^z$ interaction. By direct evaluation one can show that for the dipole-dipole interaction it is also zero.

The second group of diagrams, 3(c) represents three-spin flip-flop processes. It corresponds to a ring propagation of a spin excitation. For the dipole-dipole interaction only, due to the symmetry of interaction terms, the clockwise propagating excitation cancels the counterclockwise excitation. It is an analog of Furry's theorem.[57] An analytical form of the hyperfine-mediated contribution can be written as

$$\langle V_3^{\text{hf}} \rangle = - \sum_{\uparrow\downarrow\downarrow} B_{ij} B_{jk} B_{ki} \left\{ \frac{4it}{\omega_{ij}\omega_{ik}} - 2\frac{1 - e^{i\omega_{ik}t}}{\omega_{ik}^2 \omega_{jk}} + 2\frac{1 - e^{i\omega_{ij}t}}{\omega_{ij}^2 \omega_{jk}} \right\}, \tag{14}$$

for clusters $\{i = \uparrow, j = \downarrow, k = \downarrow\}$, where permutations of j and k spins are accounted for already. For $\{i = \downarrow, j = \uparrow, k = \uparrow\}$ clusters, one should change signs of all the frequencies ω_{ij}, ω_{ik}, and ω_{jk}.
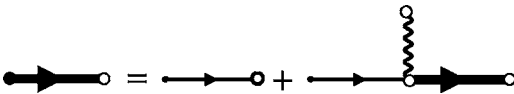
FIG. 6. Renormalization of a Green's function by the $I_i^z I_j^z$ interaction.

Diagrams of this type can be accounted for by the renormalization of Green's functions given by the Dyson equation, Fig. 6, where the renormalized Green's function (bold line) is

In the third order linked diagrams the cross-terms of the hyperfine-mediated and dipole-dipole interactions appears. For example, the ring diagram, 3(c) and the diagram shown in Fig. 3(a) with two dipole-dipole interaction lines and one hyperfine-mediated line have non-zero contributions. Because most of the third order diagrams give zero contribution to spin decoherence, the fourth order corrections need to be evaluated.

The set of the fourth order diagrams is given in Fig. 4. The only restriction on the vertices in this diagrams is that two spins i and j coupled by an interaction line should be different ($i \neq j$). Therefore, the same diagram in Fig. 4 can correspond to different number of spins in a cluster. For example, the ring diagram, 4(f) can describe excitations of two, three, and four spins. We call them two-, three-, and four-spin ring diagrams, respectively.

In the fourth order in addition to different types of renormalization of lower order diagrams 4(a)–4(e), and a ring diagram 4(f) we have contribution from the locked diagrams[40] 4(g) and 4(h). The locked diagrams contain vertices with two incoming propagators. This group compensates the time overlap of the spin pair excitations and also restricts excitations to the spin space $I^z = \pm 1/2$. The three-spin diagram 4(g) modifies a double excitation with one common spin, that appears in the expansion of the exponent V_2 term, and also correct the fourth order ring diagram with repeating indices, see Fig. 7. The two-spin diagrams 4(g) and 4(h) play a similar role for pairs with two common spins, Fig. 8. We discuss the locked diagrams in more details in Appendix B.

For spin $I = 1/2$, the two-spin diagram is compensated completely by the locked diagrams, see Fig. 8(b). The three-spin rings describe the dynamics of $i = \uparrow j = \downarrow k = \downarrow$ or $i = \downarrow j = \uparrow k = \uparrow$ clusters. After correction by the locked diagram 7(b) it corresponds to propagation of a spin excitation as
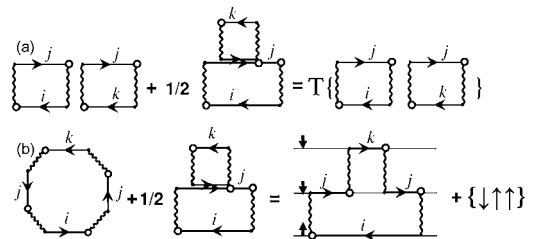
FIG. 7. Compensation of the spin excitations overlapping in time by a locked diagram. The time overlap is in one site (j).
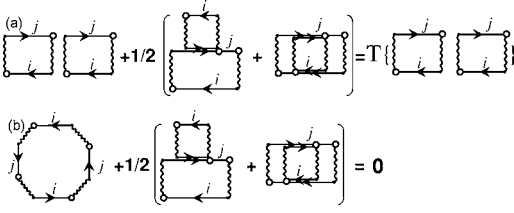
FIG. 8. Compensation of the spin excitations overlapping by a locked diagram. The time overlap is in two sites [(i) and (j)].

$i \rightarrow j \rightarrow k \rightarrow j \rightarrow i$. An analytical form of this term together with the locked diagrams 4(g) and 4(h) are given in Appendix C. A four-spin ring diagram corresponds to the dynamics of three distinct spin clusters $\uparrow\downarrow\downarrow\downarrow$, $\uparrow\downarrow\uparrow\downarrow$, and $\uparrow\uparrow\downarrow\downarrow$.

As a result, we write equation for the electron spin coherence up to the fourth order in nuclear spin-spin interactions as

$$\rho_{+-}(t) = \rho_{+-}^0 e^{-i(\omega_e + \omega_n)t} e^{\langle V_2 \rangle_n + \langle V_3 \rangle_n + \langle V_4 \rangle_n}, \tag{15}$$

where the index n denotes an initial configuration of the nuclear bath, the $\langle V_2 \rangle_n$ term (the diagram in Fig. 2) is given by Eqs. (10) and (11), the $\langle V_3 \rangle_n$ term [diagram on Fig. 3(c)] with expression given by Eq. (14) and the fourth order contribution of nuclear spin dynamics schematically shown in Fig. 9. Analytical expressions for selected terms of $\langle V_4 \rangle_n$ are in Appendix C.

The diagram series can be extended to higher orders. At each order there should be a group of diagrams renormalizing the lower orders with $I^z I^z$ terms, a group of locked diagrams that compensate the time overlap of the spin excitations in lower order clusters, as well as a group of ring diagrams.

For systems with a high concentration of nuclear spins, contributions of different diagrams to a $\langle V_k \rangle$ term can be estimated in terms of a $1/Z$ expansion,[58] where Z is the effective number of interacting spins. For example, if the last term in Fig. 9 is O(1), then the first term is O($1/Z$), second term is O($1/Z$) or O($1/Z^2$) depending on whether the diagram corresponds to a three or two-spin cluster, and the third one is O($1/Z^2$). This follows directly from the counting of a number of summands (different spin configurations) in the analytical expressions, Appendix C. If the effective number
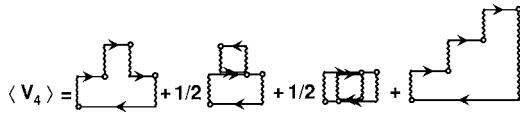
FIG. 9. The total fourth order contribution of the nuclear spin excitations to the electron spin decoherence. The first diagram corresponds to the ring propagation of the spin excitation in the three-spin clusters $\uparrow\downarrow\downarrow$ and $\downarrow\uparrow\uparrow$. The second, single-site locked, diagram corrects the overlapping of the excitations. It contributes to the spin dynamics of three- and two-spin clusters as shown in Figs. 7 and 8. The third, two-site locked, diagram corrects the overlapping of two spin excitations, Fig. 8. The last diagram describes the four-spin ring excitations in the spin clusters $\downarrow\uparrow\uparrow\uparrow$, $\uparrow\downarrow\downarrow\downarrow$, $\uparrow\downarrow\uparrow\downarrow$, and $\uparrow\uparrow\downarrow\downarrow$.

of spins interacting with a given one is large then $\langle V_4 \rangle$ term can be approximated by the last diagram in Fig. 9 only.

IV. DISCUSSION AND EXAMPLE

The equation for the free evolution of a single-electron spin coupled with a nuclear bath, Eq. (15), contains two terms. The first one is a phase factor due to the spin precession in the external field plus the Overhauser field. The second term is due to the electron-nuclear spin entanglement. In ensemble measurements, the inhomogeneous distribution of the nuclear Overhauser fields typically leads to a fast ensemble dephasing time T_2^*. This prevents a direct observation of spin decoherence in free induction decay. To remove the undesired phase factor one can use, for example, a Hahn spin-echo setup. However, it should be noted that the magnetic π pulse affects the entanglement term also.[26] All the terms evaluated in the previous section can be calculated for the echo setup straightforwardly. For example, the second order term with the dipole-dipole interaction, Fig. 2, is

$$\langle V_2^{dd} \rangle = - \sum_{i=\uparrow, j=\downarrow} (B_{ij}^{dd})^2 \left\{ 12 \frac{1 - e^{i\omega_{ij}t}}{\omega_{ij}^2} + 4 \frac{1 - e^{-i\omega_{ij}t}}{\omega_{ij}^2} \right.$$
$$\left. - 4 \frac{1 - e^{2i\omega_{ij}t}}{\omega_{ij}^2} \right\}. \tag{16}$$

All the diagrams with the hyperfine-mediated interaction are cancelled in the echo.

As an example we apply the developed technique to a model system, a phosphorous donor in a Si crystal that was first studied long ago.[56] Recently, interest in it has been renewed by the proposal for quantum computation.[59] The impurity ^{31}P is a shallow donor with the effective radius of the electron wave function $R_{eff} \sim 25$ Å.[60] Therefore, the bounded electron covers many host lattice sites. The nuclear spin bath is represented by a system of randomly distributed ^{29}Si isotopes ($I = 1/2$). The natural ^{29}Si isotope concentration is $c(^{29}\text{Si}) \approx 4.7\%$. At temperatures ~ 1 K and magnetic fields $\sim 0.1 - 1$ T the major mechanism of spin echo decay in this system is the spectral diffusion due to the coupling to the nuclear spins.[9,15]

We simulated numerically the processes shown in Figs. 2 and 9 for a single FID ($\pi/2 - t$-measurement) and spin echo setup ($\pi/2 - t/2 - \pi - t/2$-measurement). For FID we factored out the shift due to the nuclear Overhauser field and focused only on the decoherence induced by electron-nuclear dynamical entanglement. Such a calculation becomes relevant when the inhomogeneous broadening is filtered out, e.g., by the method discussed in Ref. 61. The contact hyperfine constants for the system were approximated using the effective mass theory envelope function.[60] We also assumed that the phosphorus nuclear spin contributes to the frequency shift only, because of large difference in the gyromagnetic ratios of the ^{31}P and ^{29}Si nuclei. In simulations of dipole-dipole contributions we generated an initial nuclear spin configuration in a Si lattice within a sphere of radius $5R_{eff}$ about the donor. The nuclear spin bath was assumed unpolarized. Then we selected at random a spin-up site with its surround-
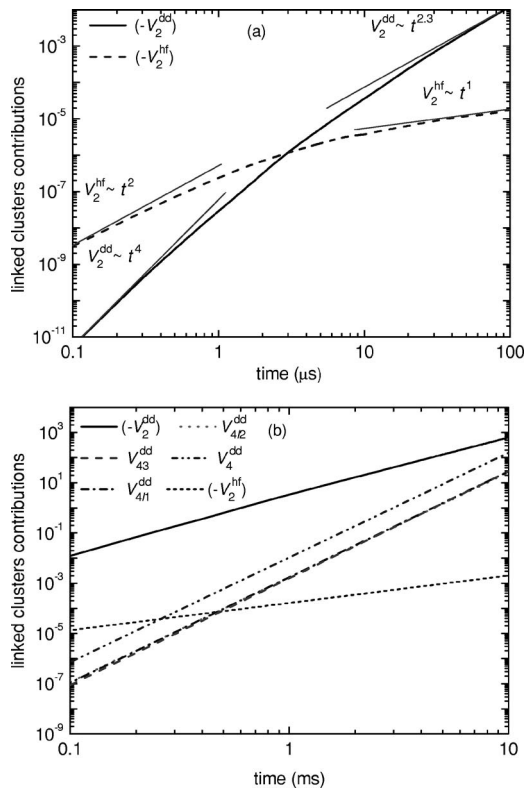
FIG. 10. Contributions of the linked clusters to the electron spin decoherence: (a) Crossover from the short-time evolution to the intermediate regime. (b) Development of the fourth order terms in the intermediate time regime. V_2 corresponds to the spin pair flip-flop process in Fig. 2; V_{43}, the three-spin excitation, the first term in Fig. 9; V_{4l1}, the single site spin locked diagram, the three-spin part of the second term in Fig. 9; V_{4l2}, correction of the overlapping of the two-spin excitations given within the brackets in Fig. 8(a), and V_4, the four-spin ring diagram, the last term in Fig. 9.

ing within a sphere of a radius $5a$, where $a = 5.43$ Å is the Si lattice constant. We calculated contributions of all possible configurations of a given central spin with its surrounding. This procedure was repeated for 10^3 times and results were normalized to the total number of spin up within the whole simulated volume. For the hyperfine-mediated interaction we averaged over 10^6 randomly generated spin configurations within the whole volume. The simulation was done for 100 different configurations of nuclear spins to account for initial state dependence of the decoherence process. The results were checked for convergence with changing parameters of the model.

For the electron spin FID the real parts of the different diagrams, Figs. 2 and 9, averaged over spatial and spin configurations of ^{29}Si are shown in Fig. 10. At very short times $t < \max\{A^{hf}\}^{-1}$ the second order terms[26] are $V_2^{hf} \sim t^2$ and $V_2^{dd} \sim t^4$. In Fig. 10(a) we show the crossover from the short-time behavior to an intermediate regime with time dependencies $V_2^{hf} \sim t^1, V_2^{dd} \sim t^{2.3}$. The dispersions in the exponent at the intermediate time scale is $\sim 5\%$ depending on the spatial positions of ^{29}Si near the P donor and the different initial configurations of nuclear spins. It also contains errors due to a finite simulated volume. In contrast to a study of the spin
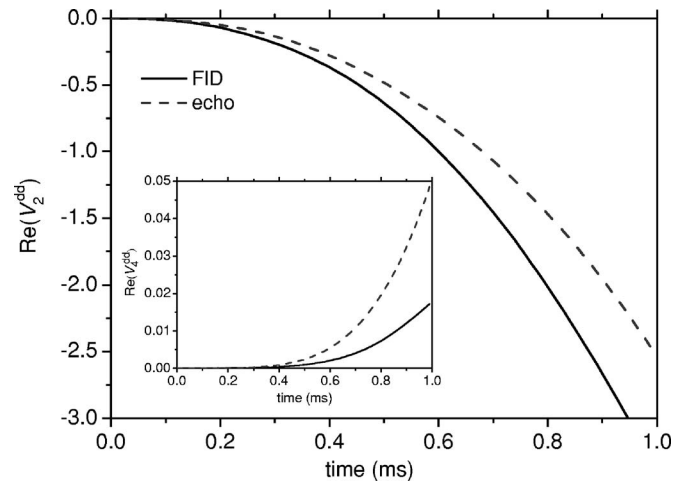
FIG. 11. Time dependence of the second and fourth (inset) order terms in the exponent. FID vs spin echo decay.

decoherence in III-V semiconductor quantum dots,[26] where the decoherence time is sufficiently short to be entirely represented by the leading powers of time in the exponent of the linked cluster expansion, the short-to-intermediate regime crossover in Si:P appears because the higher nuclear spin correlations have time to develop. For external magnetic fields $H < 0.1 - 1T$ the hyperfine-mediated term determines the short-time spin dynamics, see Fig. 10(a). However, it can be efficiently suppressed by increasing the field. Moreover, it cancels completely in the spin echo. All the dipole-dipole fourth order terms develop on the time scale of the order of several milliseconds, Fig. 10(b). However, on this time scale the electron spin coherence is completely destroyed by the $\langle V_2 \rangle$ term. This slow development of high order spin correlations is consistent with an experimental measurements.[33] At a very short times the fourth order terms are $\sim t^6$ (not shown in the figures). This dependence changes to $V_4^{dd} \sim t^{4.2}$ at a longer time scale. The contribution of the four-spin diagram is about an order of magnitude larger than the other fourth order terms. However, we abstain from attributing it to the $1/Z$ expansion because the two- and three-spin fourth order terms have powers of $1/Z$ and $1/Z^2$ but similar magnitudes. Probably, this is because the studied system of nuclear spins is dilute and Z is of order of unity. In Fig. 11 we show the total second and fourth order contributions (see inset) in the exponent for FID and spin echo setups. One can see that a π-pulse reduces the pure electron spin decoherence. This effect is an analog of suppression of the spectral diffusion considered in phenomenological models.[45,46]

For the spin echo setup we obtain the time dependence of V_2^{dd} term comparable to that was calculated in Ref. 28. However, the fourth order terms in our model do not show the nonmonotonic behavior.

We emphasize that in the Si:P system the noncontact hyperfine coupling between the electron and nuclear spins, not considered here, produces noticeable effects on electron spin dynamics.[47–49] To suppress these effects a high external magnetic field is required.[50] Moreover, in spin echo measurements on macroscopic samples the dipole-dipole interaction between electron spins causes an instantaneous diffusion.[9,62]
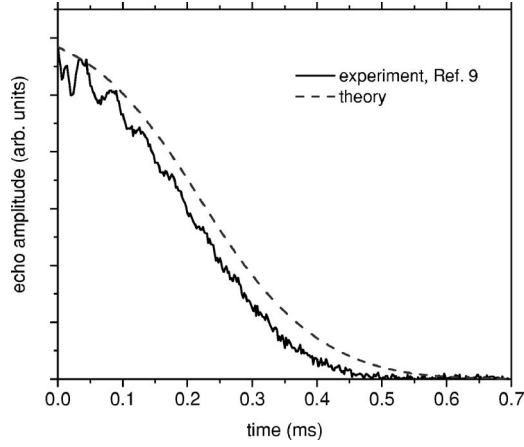
FIG. 12. Calculated spin echo decay in comparison with the experimental data.[9] Orientation of the external magnetic field is along the (100) direction.

This effect is beyond the scope of this paper on a single-electron spin. For comparison with the experimental results given in Ref. [9], we account for the instantaneous diffusion with a phenomenological exponential decay $e^{-t/t_{ID}}$. In the simulation we take the phenomenological relaxation time for instantaneous diffusion to be $t_{ID}=1.1$ ms, obtained in Ref. [9]. The results are shown in Fig. [12]. In addition to the echo modulations due to non-contact dipole-dipole hyperfine interaction observed in the experiments we still have a moderate discrepancy. Because the magnetic field used in the experiment was of the order of 0.3 T, the contribution of the hyperfine-mediated terms should be small on the time scale of the echo decay (0.1–0.5 ms). We attribute this discrepancy to the effective mass approximation for the electron wave function. More detailed comparison should be done after the echo modulation and instantaneous diffusion effects are accounted for by the theory. We leave it to future studies. The developed theory can be straightforwardly applied to study decoherence in quantum dots because we treat donor impurities and quantum dots in the same way. The only requirement is that the system Hamiltonian has the form of Eq. (1).

V. CONCLUSION

We developed a field theoretic approach to evaluate the dynamics of an electron spin interacting with a nuclear spin bath in a high field regime. The approach provides a better understanding of the difference between stochastic models of an electron spin spectral diffusion and dynamic models of spin decoherence in the presence of the nuclear spin bath. It also throws light on the problem of reversibility of spin dynamics. The approach is based on a conventional diagrammatic technique utilized in the study of Heisenberg ferromagnets. The scheme allows for an analytical evaluation of different processes contributing to the electron spin evolution. We show that the electron spin dynamics in a nuclear spin environment can be factorized into a free precession in the Overhauser field and more complex dynamics due to an electron-nuclear spin entanglement. The latter can be evaluated using a linked-cluster expansion procedure. The exact analytical expressions for second order and some high order processes are given. We show that spin decoherence of a P donor electron in a Si crystal is mostly controlled by the nuclear spin pair excitations at sufficiently low temperature and high magnetic field. Contributions of higher order processes are small and can be neglected on a time scale up to several milliseconds. A magnetic π-pulse flipping electron spin slows down the pure decoherence process. The simulated results are in fairly good agreement with experimental measurements of spin echo in macroscopic samples.

APPENDIX A

We briefly summarize the spin diagrammatic rules. Unlike Ref. [38] where the formalism was used for a statistically mixed state, our brackets correspond to a pure state specified by the initial conditions. Averaging over a thermal ensemble in our case would mix the dynamical contributions of the electron-nuclear spin entanglement with the effects of statistical distribution of the Overhauser fields. For the sake of simplicity here we assume the nuclear spin to be 1/2 but the approach can be extended to higher spins.[40]

The matrix element in Eq. (8) can be written as a product of brackets corresponding to single sites. At each nuclear spin site j with a given initial state, $|j\rangle$ $(=|\uparrow\rangle$ or $|\downarrow\rangle)$, an expectation value of time ordered spin operators

$$\langle j|T\{I^{\alpha}(t_1)I^{-}(t_2)\cdots I^{+}(t_k)I^{\beta}(t_{k+1})\cdots I^{\mu}(t_m)\}|j\rangle \quad \text{(A1)}$$

is zero if numbers of I^{+} and I^{-} operators are not equal. Otherwise, we evaluate it with the Wick's theorem.[38] Using the spin commutation relations $[I^{-},I^{+}]=-2I^{z}$ and $[I^{z},I^{+}]=I^{+}$ the bracket (A1) is transformed to the form where an operator I^{+} (I^{-} would serve as well) is in the first position

$$\langle j|I^{\alpha}(t_1)I^{+}(t)I^{\beta}(t_2)|j\rangle = \langle j|[I^{\alpha}(t_1),I^{+}(t)]I^{\beta}(t_2)|j\rangle + \langle j|I^{+}(t)I^{\alpha}(t_1)I^{\beta}(t_2)|j\rangle \quad \text{(A2)}$$

or in the last position

$$\langle j|I^{\alpha}(t_1)I^{+}(t)I^{\beta}(t_2)|j\rangle = -\langle j|I^{\alpha}(t_1),[I^{\beta}(t_2),I^{+}(t)]|j\rangle + \langle j|I^{\alpha}(t_1)I^{\beta}(t_2)I^{+}(t)|j\rangle. \quad \text{(A3)}$$

Depending on the initial state operator, I^+ is moved to the right if $|j\rangle=|\uparrow\rangle$ or to the left if $|j\rangle=|\downarrow\rangle$. After applying

$$I^+(t)|\uparrow\rangle = 0,$$

$$\langle\downarrow|I^+(t) = 0. \tag{A4}$$

a product of m spin operators is expanded into a sum of products of $m-1$ operators. This procedure is repeated until only a product of I^z operators is left. The latter term is evaluated directly. As a result, the bracket (A1) can be written in terms of all possible contractors of I^+ operator with I^- and I^z using

$$[I^\alpha(t_1), I^+(t)] = e^{i\omega(t-t_1)}[I^\alpha, I^+]_{t_1}, \tag{A5}$$

where the latter commutator is taken at time t_1. Unlike contractions of bosons or fermions a commutator of I^+ and either I^- or I^z is an operator that can be used in a next pairing. For example, in

$$\overbrace{I^+(t)\,I^z}(t_1)\,\overbrace{I^-}(t_2) \tag{A6}$$

the operator $I^+(t)$, first, is paired with $I^z(t_1)$ with the resulting $I^+(t_1)$ operator paired with $I^-(t_2)$. Another specific example of spin pairing is a locked term.[38] In

$$\overbrace{I^+(t)\,I^-}(t_1)\,\overbrace{I^+(t')\,I^-}(t_2), \tag{A7}$$

the operator $I^+(t)$ is paired with $I^-(t_1)$, then $I^+(t')$ is paired with the resulting operator $I^z(t_1)$ and finally with $I^-(t_2)$. By the locked term here we mean a term that contains an operator I^- with three contracting lines. The role of such terms in LCE we discuss in Appendix B.

In diagrams we depict I^+ vertices by points, I^- and I^z vertices by open circles and interaction terms by wavy lines. The Green's function, defined as

$$K_j(t_1, t_2) = \frac{\langle j|T\{I^+(t_1)I^-(t_2)\}|j\rangle}{(-2)\langle j|I_j^z|j\rangle} = e^{i\omega_j(t_1-t_2)}\{\delta_{j\downarrow}\theta(t_2 - t_1)$$
$$- \delta_{j\uparrow}\theta(t_1 - t_2)\}, \tag{A8}$$

is shown as a line with an arrow propagating from I^+ to I^-. An initial spin state determines the Green's function time evolution. One can see that the Green's function propagates back in time (arrow points opposite to the time arrow) if the initial spin state is $\uparrow$, and forward in time, if the state is $\downarrow$. Although the I^- and I^z vertices are depicted by same symbols there is a topological difference in their appearance in diagrams. I^z vertex can be either separated from any Green's function or connected to one incoming and one outgoing

Green function. I^- vertex can have one incoming line or two incoming and one outgoing lines. The I^+ vertex always has one outgoing Green function line. For interactions, a wavy line connecting two circles corresponds to an I^zI^z term, while a line connecting a point and a circle corresponds to an I^+I^- term.

The diagram representation can be easily translated into Green's functions. For example, the second order flip-flop term, Fig. 2 can be written as

$$\langle V_2\rangle = A \sum_{i=\uparrow, j=\downarrow} B_{ij}^2 \int_0^t dt_1 \int_0^t dt_2 K_i(t_1, t_2) K_j(t_2, t_1)(-2)^2\langle i|I_i^z|i\rangle$$
$$\times \langle j|I_j^z|j\rangle. \tag{A9}$$

The coefficient A in front of the sum accounts for the number of equivalent diagrams. In the particular case it is equal one. The coefficient $(-2)^2$ appears from two contractions of I^+I^- operators. Analytical expressions for diagrams are dependent on the initial spin states. For example, pairs $\uparrow\uparrow$ or $\downarrow\downarrow$ give zero contribution to $\langle V_2\rangle$ term, see Fig. 2, while the contributions of $\uparrow\downarrow$ and $\downarrow\uparrow$ pairs are equal. We usually omit this configuration dependence in graphic representation. For example, three spin diagram, Fig. 3(c) corresponds to two possible spin clusters $\uparrow\downarrow\downarrow$ and $\downarrow\uparrow\uparrow$ (Fig. 13) that have different analytical expressions. In general, one can distinguish between configurations that can be transformed to each other by changing order in spin counting or by rotation or inversion of the coordinate system and configurations that are distinct. The first type of configurations are $\uparrow\downarrow\downarrow$ and $\downarrow\uparrow\downarrow$. If we start counting the spins from the $\uparrow$ site these configurations are the same, and they have equal analytical expressions. In the case given in Fig. 13 the two spin configurations are connected by the inversion operation. An analytical form of the second diagram at the right hand side can be obtained by changing signs at all frequencies ω in an expression for the first diagram. Distinct configurations are, for example, $\uparrow\downarrow\uparrow\downarrow$ and $\uparrow\uparrow\downarrow\downarrow$ contributing to the same forth order ring diagram, Fig. 3(f).

APPENDIX B

Here we consider in more details a physical origin of the locked terms in LCE. For the sake of simplicity we assume that the interaction is

$$V(t) = \sum_{ij} B_{ij}I_i^+(t)I_j^-(t), \tag{B1}$$

and we evaluate

$$\langle n|T\{e^{-i\int_0^t V(t')dt'}\}|n\rangle$$
$$= \langle n|1 + (-i)\int_0^t V(t')dt'$$
$$+ (-i)^2/2! \int_0^t \int_0^t T\{V(t')V(t'')\}dt'\,dt'' + \cdots|n\rangle, \tag{B2}$$

where n denotes a spin configuration. The locked diagrams appear in the fourth order contribution and correspond to two-spin and three-spin excitations. A two-spin-fourth-order correction can be written as

$$3(-i)^4/4! \sum_{ij} B_{ij}^4 \int_0^t \int_0^t \int_0^t \int_0^t T\{\langle i|I_i^+(t_1)I_i^-(t_2)I_i^+(t_3)I_i^-(t_4)|i\rangle$$

$$\times \langle j|I_j^-(t_1)I_j^+(t_2)I_j^-(t_3)I_j^+(t_4)|j\rangle\}dt_1 dt_2 dt_3 dt_4, \qquad (B3)$$

where we have separated operators corresponding to different spins. The coefficient 3 in front of Eq. (B3) accounts for possible choices of i and j. Equation (B3) is nonzero only if $i=\uparrow$, $j=\downarrow$ (for $i=\downarrow$, $j=\uparrow$ we just change order in counting of spins and get the same configuration). The only possible time ordering in this case is $t_1 > t_2 > t_3 > t_4$ or $t_1 > t_4 > t_3 > t_2$. The integrand for both sets of time ordering is the same and equal $e^{i\omega_{ij}(t_1-t_2+t_3-t_4)}$. The same result we can obtain with the spin diagram technique and diagram equations given in Fig. 8. Firstly, we expand the time ordered product of the spin operators in Eq. (B3) in terms of all possible contractors as discussed in Appendix A. There are two unlinked terms of the form

$$I_i^+(t_1)I_i^-(t_2)I_i^+(t_3)I_i^-(t_4)I_j^-(t_1)I_j^+(t_2)I_j^-(t_3)I_j^+(t_4), \qquad (B4)$$

two linked terms corresponding to the ring diagram, given in Fig. 4(f)

$$I_i^+(t_1)I_i^-(t_2)I_i^+(t_3)I_i^-(t_4)I_j^-(t_1)I_j^+(t_2)I_j^-(t_3)I_j^+(t_4), \qquad (B5)$$

eight single-site locked terms, Fig. 4(g), of the form

$$I_i^+(t_1)I_i^-(t_2)I_i^+(t_3)I_i^-(t_4)I_j^-(t_1)I_j^+(t_2)I_j^-(t_3)I_j^+(t_4), \qquad (B6)$$

and four two-sites locked terms, Fig. 4(h)

$$I_i^+(t_1)I_i^-(t_2)I_i^+(t_3)I_i^-(t_4)I_j^-(t_1)I_j^+(t_2)I_j^-(t_3)I_j^+(t_4). \qquad (B7)$$

Equation (B4) corresponds to the series expansion of the second order contribution. However, it allows some non-physical states, because the contractions in it specify time ordering $t_1 > t_2$ and $t_3 > t_4$ only. By direct evaluation, one can show that the locked terms, (B6) and (B7), modify it according to the diagram equation given in Fig. 8(a) to get a correct time ordering $t_1 > t_2 > t_3 > t_4$. It is a correction of overlapping
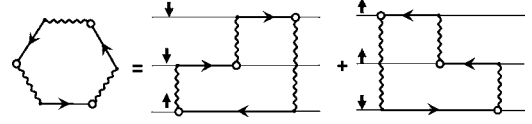
FIG. 13. Representation of a third order diagram using the cluster configurations.

of spin excitations discussed in Refs. 26 and 28. The locked diagram is the price we pay to obtain LCE for spins. This shows that the procedure to get an exponential form of a qubit decoherence is not as simple as it was suggested in Ref. 28.

APPENDIX C

Here we provide explicit analytical expressions for two and three spin diagrams given in Fig. 9. The first term is denoted as V_{43}, the three-spin part of the second term is V_{41l} and the two-spin part of the second term plus the third term is V_{42l}. The coefficients $1/2$ indicated in Fig. 9 are understood. The analytical expression for the last, four-spin, diagram is lengthy though its evaluation is not complicated. We give terms for the hyperfine-mediated and dipole-dipole interactions separately.

Contributions of the hyperfine-mediated interaction are as follows.

(a) The three spin ring with the overlap corrected,

$$\langle V_{43}^{\text{hf}}\rangle = -\sum_{\uparrow\downarrow\downarrow} B_{ij}^2 B_{jk}^2 \left\{ 2it\left(\frac{1}{\omega_{ij}^2\omega_{ik}} + \frac{e^{2i\omega_{ij}t}}{\omega_{ij}^2\omega_{jk}}\right) + 2\frac{1-e^{2i\omega_{ij}t}}{\omega_{ij}^3\omega_{jk}} \right.$$

$$\left. + \frac{1-e^{2i\omega_{ik}t}}{\omega_{ik}^2\omega_{jk}^2} - \frac{1-e^{2i\omega_{ij}t}}{\omega_{ij}^2\omega_{jk}^2} \right\}. \qquad (C1)$$

(b) The diagram compensating a single site overlap

$$\langle V_{4l1}^{\text{hf}}\rangle = 2\sum_{\uparrow\downarrow\downarrow} B_{ij}^2 B_{ik}^2 \left\{ 2it\frac{1+e^{2i\omega_{ij}t}}{\omega_{ij}^2\omega_{ik}} \right.$$

$$\left. + \frac{(2\omega_{ik}^2 - \omega_{ij}\omega_{ik} + \omega_{ij}^2)(1-e^{2i\omega_{ij}t})}{\omega_{ij}^3\omega_{ik}^2\omega_{jk}} - \frac{1-e^{2i(\omega_{ik}+\omega_{ij})t}}{2\omega_{ik}^2\omega_{ij}^2} \right\}$$

$$+ \{j \leftrightarrow k\}. \qquad (C2)$$

(c) The compensation of a double site time overlap (two diagrams),

$$\langle V_{4l2}^{\text{hf}}\rangle = -\sum_{\uparrow\downarrow} B_{ij}^4 \left\{ -2it\frac{1+e^{2i\omega_{ij}t}}{\omega_{ij}^3} + \frac{e^{4i\omega_{ij}t}+2e^{2i\omega_{ij}t}-5}{2\omega_{ij}^4} \right\}. \qquad (C3)$$

The same diagrams for the dipole-dipole interaction only have the following expression.

(a) The three spin ring with the overlap corrected

$$\langle V_{43}^{\mathrm{dd}}\rangle = -\sum_{\uparrow\downarrow\downarrow} B_{ij}^2 B_{jk}^2 \left\{ 2it\left(\frac{2\omega_{ik}-\omega_{ij}}{\omega_{ij}^2\omega_{ik}\omega_{jk}} - \frac{(1-e^{i\omega_{ij}t})^2}{\omega_{ij}^2\omega_{jk}} \right) + 4\frac{(\omega_{ij}^2-2\omega_{jk}^2)e^{i\omega_{ij}t}}{\omega_{ij}^3\omega_{ik}\omega_{jk}^2} - \frac{e^{2i\omega_{ik}t}}{\omega_{ik}^2\omega_{jk}^2} - 4\frac{e^{i\omega_{ik}t}}{\omega_{ij}\omega_{ik}\omega_{jk}^2} - \frac{(3\omega_{ij}-2\omega_{jk})e^{2i\omega_{ij}t}}{\omega_{ij}^3\omega_{jk}^2} \right.$$
$$\left. + 4\frac{e^{i(\omega_{ik}+\omega_{ij})t}}{\omega_{ij}\omega_{ik}\omega_{jk}^2} + \frac{\omega_{ij}+6\omega_{ik}}{\omega_{ik}^2\omega_{ij}^3} \right\}. \tag{C4}$$

(b) The diagram compensating a single site overlap

$$\langle V_{4l1}^{\mathrm{dd}}\rangle = 2\sum_{\uparrow\downarrow\downarrow} B_{ij}^2 B_{ik}^2 \left\{ 2it\frac{2-(1-e^{i\omega_{ij}t})^2}{\omega_{ij}^2\omega_{ik}} - \frac{12e^{i(\omega_{ij}+\omega_{ik})t}+e^{2i(\omega_{ij}+\omega_{ik})t}-8e^{i(\omega_{ik}+2\omega_{ij})}}{2\omega_{ij}^2\omega_{ik}^2} \right.$$
$$\left. + \frac{8(\omega_{ij}^2+\omega_{ik}^2-\omega_{ij}\omega_{ik})e^{i\omega_{ij}t}-(2\omega_{ik}^2+3\omega_{ij}^2-3\omega_{ij}\omega_{ik})e^{2i\omega_{ij}t}}{\omega_{ij}^3\omega_{ik}^2(\omega_{ij}-\omega_{ik})} + \frac{6\omega_{ij}^2+\omega_{ij}\omega_{ik}+6\omega_{ik}^2}{2\omega_{ij}^3 a_{ik}^3} \right\} + \{j\leftrightarrow k\}. \tag{C5}$$

(c) The compensation of a double site time overlap

$$\langle V_{4l2}^{\mathrm{dd}}\rangle = -\sum_{\uparrow\downarrow} B_{ij}^4 \left\{ 2it\frac{2(1-e^{i\omega_{ij}t})^2-3}{\omega_{ij}^3} + \frac{e^{4i\omega_{ij}t}-8e^{3i\omega_{ij}t}+12e^{2i\omega_{ij}t}+8e^{i\omega_{ij}t}-13}{2\omega_{ij}^4} \right\}. \tag{C6}$$

In the equations, $\{j\leftrightarrow k\}$ means the same expression with interchanged j and k indexes.

*Electronic address: ssaikin@physics.ucsd.edu; http// www.physics.ucsd.edu/~ssaikin

†Present address: Department of Physics, The University of Texas, Austin, Texas 78712-0264

[1] A. Schweiger and G. Jeschke, *Principles of Pulse Electron Paramagnetic Resonance* (Oxford University press, New York, 2001).

[2] M. A. Nielsen and I. L. Chuang, *Quantum Computation and Quantum Information* (Cambridge University Press, Cambridge, 2000).

[3] S. A. Wolf, A. Y. Chtchelkanova, and D. M. Treger, IBM J. Res. Dev. **50**, 101 (2006).

[4] K. Ono and S. Tarucha, Phys. Rev. Lett. **92**, 256803 (2004).

[5] M. V. Gurudev Dutt, J. Cheng, B. Li, X. Xu, X. Li, P. R. Berman, D. G. Steel, A. S. Bracker, D. Gammon, S. E. Economou, R.-B. Liu, and L. J. Sham, Phys. Rev. Lett. **94**, 227403 (2005).

[6] A. C. Johnson, J. R. Petta, J. M. Taylor, A. Yacoby, M. D. Lukin, C. M. Marcus, M. P. Hanson, and A. C. Gossard, Nature (London) **435**, 925 (2005).

[7] P.-F. Braun, X. Marie, L. Lombez, B. Urbaszek, T. Amand, P. Renucci, V. K. Kalevich, K. V. Kavokin, O. Krebs, P. Voisin, and Y. Masumoto, Phys. Rev. Lett. **94**, 116601 (2005).

[8] R. Giraud, W. Wernsdorfer, A. M. Tkachuk, D. Mailly, and B. Barbara, Phys. Rev. Lett. **87**, 057203 (2001).

[9] A. M. Tyryshkin, J. J. L. Morton, S. C. Benjamin, A. Ardavan, G. A. D. Briggs, J. W. Ager, and S. A. Lyon, J. Phys.: Condens. Matter **18**, S783 (2006).

[10] L. Viola, E. Knill, and S. Lloyd, Phys. Rev. Lett. **82**, 2417 (1999).

[11] A. M. Steane, Phys. Rev. A **68**, 042322 (2003).

[12] D. Mozyrsky, Sh. Kogan, V. N. Gorshkov, and G. P. Berman, Phys. Rev. B **65**, 245213 (2002), S. I. Erlingsson and Y. V. Nazarov, *ibid.* **66**, 155327 (2002).

[13] A. V. Khaetskii, D. Loss, and L. Glazman, Phys. Rev. Lett. **88**, 186802 (2002).

[14] J. R. Klauder and P. W. Anderson, Phys. Rev. **125**, 912 (1962).

[15] M. Chiba and A. Hirai, J. Phys. Soc. Jpn. **33**, 730 (1972).

[16] K. M. Salikhov, A. G. Semenov, and Yu. D. Tsvetkov, *Electron Spin Echo and its Application* (Nauka, Novosibirsk, 1976) [in Russian].

[17] N. Prokof'ev and P. C. E. Stamp, Rep. Prog. Phys. **63**, 669 (2000).

[18] I. A. Merkulov, Al. L. Efros, and M. Rosen, Phys. Rev. B **65**, 205309 (2002).

[19] S. Saykin, D. Mozyrsky, and V. Privman, Nano Lett. **2**, 651 (2002).

[20] J. Schliemann, A. Khaetskii, and D. Loss, J. Phys.: Condens. Matter **15**, R1809 (2003).

[21] Yu. V. Pershin and V. Privman, Nano Lett. **3**, 695 (2003).

[22] S. I. Erlingsson and Y. V. Nazarov, Phys. Rev. B **70**, 205327 (2004).

[23] W. A. Coish and D. Loss, Phys. Rev. B **70**, 195340 (2004).

[24] W. M. Witzel, R. de Sousa, and S. Das Sarma, Phys. Rev. B **72**, 161306(R) (2005).

[25] N. Shenvi, R. de Sousa, and K. B. Whaley, Phys. Rev. B **71**, 144419 (2005).

[26] W. Yao, R.-B. Liu, and L. J. Sham, Phys. Rev. B **74**, 195301 (2006).

[27] K. A. Al-Hassanieh, V. V. Dobrovitski, E. Dagotto, and B. N. Harmon, Phys. Rev. Lett. **97**, 037204 (2006).

[28] W. M. Witzel and S. Das Sarma, Phys. Rev. B **74**, 035322 (2006).

[29] W. Yao, R.-B. Liu, and L. J. Sham, Phys. Rev. Lett. **98**, 077602 (2007).

[30] C. Deng and X. Hu, Phys. Rev. B **73**, 241303(R) (2006).

[31] V. Privman, J. Stat. Phys. **110**, 957 (2003).

[32] W.-K. Rhim, A. Pines, and J. S. Waugh, Phys. Rev. Lett. **25**, 218 (1970).

[33] H. Cho, T. D. Ladd, J. Baugh, D. G. Cory, and C. Ramanathan,

Phys. Rev. B **72**, 054427 (2005).

[34] R. B. Stinchcombe, G. Horwitz, F. Englert, and R. Brout, Phys. Rev. **130**, 155 (1963).

[35] B. Giovannini and S. Koide, Prog. Theor. Phys. **34**, 705 (1965).

[36] Y. L. Wang, S. Shtrikman, and H. Callen, Phys. Rev. **148**, 419 (1966).

[37] V. G. Vaks, A. I. Larkin, and S. A. Pikin, Sov. Phys. JETP **53**, 1089 (1967) [Sov. Phys. JETP **26**, 647 (1968)].

[38] Yu. A. Izyumov and F. A. Kassan-Ogly, Fiz. Met. Metalloved. **26**, 385 (1968); **30**, 225 (1970).

[39] Yu. A. Izyumov, F. A. Kassan-Ogly, and Yu. N. Scryabin, *Field Methods in Theory of Ferromagnetism* (*Fiziko-Matematicheskaya Literatura*, Moscow, 1974) [in Russian].

[40] David Hsing-Yen Yang and Yung-Li Wang, Phys. Rev. B **10**, 4714 (1974).

[41] V. G. Baryakhtar, V. N. Krivoruchko, and D. A. Yablonskii, Theor. Math. Phys. **56**, 149 (1983) [Theor. Math. Phys. **56**, 731 (1983)].

[42] V. G. Baryakhtar, V. N. Krivoruchko, and D. A. Yablonskii, *Green Functions in the Theory of Magnetism* (Nauk-dumka, Kiev, 1984) [in Russian].

[43] J. L. Ivey and R. L. Mieher, Phys. Rev. B **11**, 849 (1975).

[44] S. Lee, P. von Allmen, F. Oyafuso, G. Klimeck, and K. B. Whaley, J. Appl. Phys. **97**, 043706 (2005).

[45] C. P. Slichter, *Principles of Magnetic Resonance* (Springer-Verlag, Berlin, 1980).

[46] L. G. Rowan, E. L. Hahn, and W. B. Mims, Phys. Rev. **137**, A61 (1965).

[47] M. Fanciulli, P. Hofer, and A. Ponti, Physica B **340-342**, 895 (2003).

[48] J. J. L. Morton, A. M. Tyryshkin, A. Ardavan, K. Porfyrakis, S. A. Lyon, and G. A. D. Briggs, J. Chem. Phys. **122**, 174504 (2005).

[49] E. Abe, K. M. Itoh, J. Isoya, and S. Yamasaki, Phys. Rev. B **70**, 033204 (2004).

[50] S. Saikin and L. Fedichkin, Phys. Rev. B **67**, 161302(R) (2003).

[51] N. G. van Kampen, *Stochastic Processes in Physics and Chemistry* (Elsevier North-Holland, Amsterdam 2001).

[52] G. D. Mahan, *Many-Particle Physics* (Kluwer Academic/Plenum Publishers, New York, 2000).

[53] A. A. Abrikosov, L. P. Gorkov, and I. E. Dzyaloshinski, *Methods of Quantum Field Theory in Statistical Physics* (Prentice-Hall, Englewood Cliffs, NJ, 1963).

[54] L. P. Kadanoff and G. Baym, *Quantum Statistical Mechanics; Green's Function Methods in Equilibrium and Nonequilibrium Problems* (Benjamin, New York, 1962).

[55] L. V. Keldysh, Sov. Phys. JETP **20**, 1018 (1965), [Sov. Phys. JETP **47**, 1515 (1964)].

[56] G. Feher, Phys. Rev. **114**, 1219 (1959).

[57] W. H. Furry, Phys. Rev. **51**, 125 (1937).

[58] R. Brout, Phys. Rev. **118**, 1009 (1960).

[59] B. E. Kane, Nature (London) **393**, 133 (1998).

[60] W. Kohn, *Shallow Impurity States in Silicon and Germanium*, Solid State Physics V (Academic Press, Inc., New York, 1957), p. 257.

[61] D. Stepanenko, G. Burkard, G. Giedke, and A. Imamoglu, Phys. Rev. Lett. **96**, 136401 (2006).

[62] A. Ferretti, M. Fanciulli, A. Ponti, and A. Schweiger, Phys. Rev. B **72**, 235201 (2005).